CRACK PATH SELECTION IN A BRITTLE ADHESIVE LAYER

NORMAN A. FLECK

Engineering Department, Cambridge University, Cambridge CB2 1PZ, U.K.

JOHN W. HUTCHINSON

Division of Applied Sciences, Pierce Hall, Harvard University, Cambridge, MA 02138, U.S.A.

and

ZHIGANG SUO

Department of Mechanical Engineering, University of California,
Santa Barbara, CA 93106, U.S.A.

Abstract—Cracks in a brittle adhesive layer joining two substrates have been observed to propagate in a variety of ways, including straight or wavy paths within the adhesive layer, paths along one of the interfaces, and paths alternating from interface to interface through the layer. The effective toughness of the joint depends on the nature of the path. An asymptotic elasticity problem is analyzed in this paper which allows one to predict whether a straight crack path can occur within a brittle adhesive layer. In the asymptotic problem, an adhesive layer between two semi-infinite blocks contains a semi-infinite straight crack. The joint is loaded remotely by the first three terms of the stress field expansion for a cracked homogeneous solid, parameterized by stress intensity factors K_I^∞ and K_{II}^∞, and the non-singular stress acting parallel to the crack, T^∞. These are the apparent, or applied, load factors determined from the analysis of an actual specimen by neglecting the presence of the layer. Also present is a residual stress in the adhesive layer. We calculate the local stress intensity factors, K_I and K_{II}, and the non-singular stress, T, associated with the field at the tip of the crack in the layer in terms of the corresponding applied quantities and the residual stress. A necessary condition for the existence of a straight path within the layer is the location of a path with $K_{II} = 0$. Such a path will only be stable (i.e. grow in a straight, non-wavy manner) if $T < 0$. Our analysis provides the location of the crack in terms of the combination of applied intensity factors and the mismatch in elastic moduli between the layer and the adjoining material. Stability depends on the residual stress and T^∞, as well as on the moduli mismatch. For a compliant adhesive with predominant applied mode I loading, the crack will tend to run stably within the layer unless T^∞ and the residual stress are positive and relatively large.

INTRODUCTION

The subject of the present paper is to study cracking confined to *brittle* adhesive layers. In the present context, an adhesive layer is said to be brittle if the size of the plastic zone around a crack tip, r_p, is small compared with the layer thickness, H, namely,

$$r_p \cong \frac{1}{3\pi}\left(\frac{K_{Ic}}{\sigma_Y}\right)^2 < \frac{H}{25} \tag{1}$$

where K_{Ic} is the fracture toughness and σ_Y the yield stress of the bulk adhesive, respectively. Examples of adhesives that have been used to join ceramics are given in Table 1. The layer thickness, H, is typically of the order of 100 μm. Thus, judged from eqn (1), epoxy and glass are brittle adhesives, while aluminum is ductile.

Wang and Suo (1990) have measured the fracture energy of an epoxy layer joining two aluminum alloy half-disks using sandwiched Brazil nut specimens. When the base specimen is subjected to predominantly mode I load, they observed that the crack often runs *within* the epoxy layer rather than along the epoxy–aluminum interface, although the fracture energy for epoxy is two or more times higher than that for the particular epoxy/aluminum interface. Such a peculiar phenomenon has also been observed by other authors [e.g. Cao and Evans (1989) and Cao (1989)]. As a consequence, the measured

Table 1. Plastic zone size of several adhesives

Adhesive	K_{1c} (MPa m$^{1/2}$)	σ_Y (MPa)	r_p (μm)
epoxy	0.6	85	5
glass	0.7		$\cong 0$
aluminum	30	100	3×10^4

effective fracture energy of the joint G_c versus the combination of remote loads has the discontinuous characteristics of Fig. 1. For predominantly mode I loading with only a small component of mode II, the fracture occurs within the epoxy layer, and the measured G_c is the fracture energy of the bulk epoxy, G_{1c}. When the mode II component is sufficiently large, typically $\tan^{-1}(K_{II}^\infty/K_I^\infty) \geqslant 15°$, the crack runs along the epoxy/aluminum interface and the measured G_c is the mode-dependent interfacial fracture energy.

The issues of crack path selection and stability can be addressed in terms of the asymptotic stress field around the crack tip. Let (r, θ) be polar coordinates centered at the tip of a traction-free crack in a homogeneous isotropic solid. The Williams asymptotic expansion of stresses is

$$\begin{bmatrix} \sigma_{xx} & \sigma_{xy} \\ \sigma_{xy} & \sigma_{yy} \end{bmatrix} = \frac{K_1}{\sqrt{2\pi r}} \begin{bmatrix} \tilde{\sigma}_{xx}^I(\theta) & \tilde{\sigma}_{xy}^I(\theta) \\ \tilde{\sigma}_{xy}^I(\theta) & \tilde{\sigma}_{yy}^I(\theta) \end{bmatrix}$$

$$+ \frac{K_{II}}{\sqrt{2\pi r}} \begin{bmatrix} \tilde{\sigma}_{xx}^{II}(\theta) & \tilde{\sigma}_{xy}^{II}(\theta) \\ \tilde{\sigma}_{xy}^{II}(\theta) & \tilde{\sigma}_{yy}^{II}(\theta) \end{bmatrix} + \begin{bmatrix} T & 0 \\ 0 & 0 \end{bmatrix} + O(\sqrt{r}) \quad (2)$$

where K_I and K_{II} are stress intensity factors of opening and shearing modes, respectively, and the constant term T is a stress acting parallel to the crack plane. The nondimensional θ-dependent functions are normalized so that the stresses ahead of the crack tip ($\theta = 0$) are given by

$$\begin{bmatrix} \sigma_{xx} & \sigma_{xy} \\ \sigma_{xy} & \sigma_{yy} \end{bmatrix} = \frac{K_1}{\sqrt{2\pi r}} \begin{bmatrix} 1 & 0 \\ 0 & 1 \end{bmatrix} + \frac{K_{II}}{\sqrt{2\pi r}} \begin{bmatrix} 0 & 1 \\ 1 & 0 \end{bmatrix} + \begin{bmatrix} T & 0 \\ 0 & 0 \end{bmatrix} + O(\sqrt{r}). \quad (2a)$$

It is an experimentally established fact that a crack advancing continuously in an isotropic homogeneous brittle solid selects a trajectory where $K_{II} = 0$. Symmetry dictates that a crack along the centerline of a layer joining identical materials and subject to remote pure mode I loading will be under pure mode I locally. When the base specimen carries some mode II in addition to mode I, the crack may find a pure mode I path *off* the centerline.
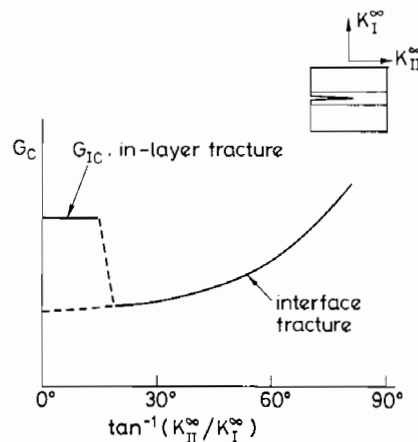

Fig. 1. Schematic of observed toughness of an epoxy layer between aluminum substrates, from tests of Wang and Suo (1989).

According to Cotterell and Rice (1980), a straight crack advancing with $K_{II} = 0$ is directionally stable if $T < 0$ and unstable if $T > 0$. This assertion may be interpreted in the following way. If the straight path of a mode I crack is perturbed as the crack tip advances due to some micro-heterogeneity, a positive T-value will cause the crack to veer away from the straight trajectory while a negative T-value will pull the path back in line. In other words, a straight path within the adhesive layer can only exist if a pure mode I crack path exists *and* if its tip has $T < 0$. The present analysis permits this assessment to be made. In addition, we discuss the behavior of a straight crack positioned away from the pure mode I trajectory to evaluate whether it kinks toward the pure mode I trajectory or towards the interface.

AN ELASTICITY PROBLEM AND ITS SOLUTION

An elasticity problem that addresses the above issues is introduced in Fig. 2. An adhesive layer of thickness H is sandwiched between blocks of an identical solid. Each solid is taken to be isotropic, homogeneous and elastic, with shear modulus and Poisson's ratio (μ_a, ν_a) for the adhesive, and (μ_s, ν_s) for the substrates. The plane strain problem is considered since the out-of-plane dimension of the joint is assumed to be much larger than the layer thickness. A crack lies parallel to the interfaces and is located within the layer at a distance c above the lower interface. We consider the asymptotic problem wherein the crack is semi-infinite and the blocks are semi-infinite as well. This is appropriate when the adhesive is very thin compared to other in-plane lengths in a given specimen or geometry.

The non-dimensional parameters that characterize this bimaterial structure are the relative crack depth, c/H, and the Dundurs (1969) *elastic mismatch parameters*

$$\alpha = \frac{(1-\nu_a)/\mu_a - (1-\nu_s)/\mu_s}{(1-\nu_a)/\mu_a + (1-\nu_s)/\mu_s}, \quad \beta = \frac{1}{2} \frac{(1-2\nu_a)/\mu_a - (1-2\nu_s)/\mu_s}{(1-\nu_a)/\mu_a + (1-\nu_s)/\mu_s}. \tag{3}$$

Two other combinations appear frequently and are related to Dundurs' parameters by:

$$\frac{\bar{E}_a}{\bar{E}_s} = \frac{1-\alpha}{1+\alpha}, \quad \varepsilon = \frac{1}{2\pi} \ln \frac{1-\beta}{1+\beta}. \tag{3a}$$

Here $\bar{E} = 2\mu/(1-\nu)$ is the plane strain tensile modulus, and ε is the oscillatory index responsible for various pathological behaviors in linear elasticity solutions for bimaterial interface cracks. Observe that $\beta = \alpha/4$ when $\nu_s = \nu_a = 1/3$, and that values of α and β for many bimaterials are clustered near the line $\beta = \alpha/4$ on the (α, β) plane (Suga *et al.*, 1988). For this reason, solutions in this paper are sometimes plotted using only one elastic mismatch constant α, with the understanding that $\beta = \alpha/4$.

There are four independent load-like quantities in the problem. A residual stress, σ^0, exists in the adhesive due to thermal mismatch or other sources. Let K_I^∞, K_{II}^∞ and T^∞ denote
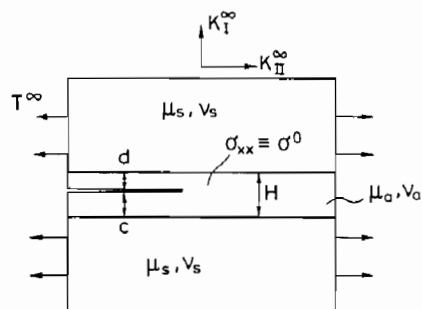
Fig. 2. The elasticity problem.

the crack-tip quantities evaluated for the actual specimen or geometry neglecting the presence of the layer. We refer to these as the applied loads determined from the homogeneous base specimen. They are related to the applied loads and geometries as can be found in Tada *et al.* (1985) for K values and Larsson and Carlsson (1973) for T values. The remote field in the asymptotic problem in Fig. 2 is specified by K_I^∞, K_{II}^∞, T^∞ and σ^0. The solution of the elasticity problem provides the local K_I, K_{II} and T at the crack tip within the layer in terms of the remote load-like quantities. Note that the local quantities are different from the remote ones because of elastic dissimilarity and the residual stress. A general integral equation formulation for cracks in layered composites has been presented by Erdogan and Gupta (1971). The solution procedure we adopt follows directly from Suo and Hutchinson (1989), and is described in detail in Appendices A and B.

The local T-stress depends linearly on all four loading parameters. Dimensional and compatibility arguments lead to

$$T = \frac{1-\alpha}{1+\alpha} T^\infty + \sigma^0 + c_1 \frac{K_I^\infty}{\sqrt{H}} + c_{II} \frac{K_{II}^\infty}{\sqrt{H}} \tag{4}$$

where the coefficient of T^∞ is readily evaluated and σ^0 denotes the σ_{xx} component of residual stress pre-existing in the layer. The two non-dimensional functions, $c_1(c/H, \alpha, \beta)$ and $c_{II}(c/H, \alpha, \beta)$, were computed as detailed in Appendices A and B and are tabulated in Appendix C.

Consider the local stress intensity factors next. It is seen that both σ^0 and T^∞ do not induce a stress intensity at the crack tip by the following argument: when no crack is present in the layer, σ^0 and T^∞ cause no traction on any plane parallel to the layer. One concludes that the local (K_I, K_{II}) depend only on the remote loads K_I^∞, K_{II}^∞. The two sets are connected by the energy release rate due to conservation of the J-integral, namely

$$G = J = \frac{1}{\bar{E}_a}(K_I^2 + K_{II}^2) = \frac{1}{\bar{E}_s}[(K_I^\infty)^2 + (K_{II}^\infty)^2]. \tag{5}$$

Algebraically, eqn (5) is equivalent to

$$K_I = \left(\frac{1-\alpha}{1+\alpha}\right)^{1/2} (K_I^\infty \cos\phi - K_{II}^\infty \sin\phi)$$

$$K_{II} = \left(\frac{1-\alpha}{1+\alpha}\right)^{1/2} (K_I^\infty \sin\phi + K_{II}^\infty \cos\phi) \tag{6a}$$

or

$$(K_I + iK_{II}) = \left(\frac{1-\alpha}{1+\alpha}\right)^{1/2} (K_I^\infty + iK_{II}^\infty) e^{i\phi} \tag{6b}$$

where ϕ can be interpreted as a phase angle shift between the remote and the local stress intensities, $\phi = \tan^{-1}(K_{II}/K_I) - \tan^{-1}(K_{II}^\infty/K_I^\infty)$. Dimensional considerations and linearity dictate that ϕ is only a function of structure, i.e. $\phi = \phi(c/H, \alpha, \beta)$. This functional dependence has also been computed and is given below.

Two solutions exist in the literature which enable us to obtain ϕ when c/H is sufficiently small or sufficiently close to unity. A sub-interface crack very close to the interface has been analyzed by Hutchinson *et al.* (1987). The local K_I and K_{II} can be expressed in terms of the complex stress-intensity factor K for the corresponding problem where the crack lies on the interface. The connection between the two sets of intensity factors when the crack lies just below the interface is

$$K_I + iK_{II} = \left(\frac{1-\beta^2}{1+\alpha}\right)^{1/2} K(H-c)^{i\varepsilon} e^{i\phi_H}. \tag{7}$$

where the function $\phi_H(a, \beta)$ is given in Hutchinson *et al.* (1987). The complex stress intensity factor K when the crack lies *in* the upper interface of the sandwich structure is solved in Suo and Hutchinson (1989) and is given by

$$K = \left(\frac{1-a}{1-\beta^2}\right)^{1/2} (K_I^\infty + iK_{II}^\infty) H^{-i\varepsilon} e^{i\omega(\alpha,\beta)} \tag{8}$$

where the function $\omega(\alpha,\beta)$ is tabulated in Suo and Hutchinson (1989). Eliminating K from the above two formulae, one obtains the connection between the local and remote stress intensity factors which is valid when $(H-c)/H$ is sufficiently small:

$$K_I + iK_{II} = \left(\frac{1-\alpha}{1+\alpha}\right)^{1/2} (K_I^\infty + iK_{II}^\infty) \left(\frac{H-c}{H}\right)^{i\varepsilon} e^{i(\phi_H+\omega)}. \tag{9a}$$

The corresponding formula for c/H near zero is

$$K_I + iK_{II} = \left(\frac{1-\alpha}{1+\alpha}\right)^{1/2} (K_I^\infty + K_{II}^\infty) \left(\frac{c}{H}\right)^{i\varepsilon} e^{-i(\phi_H+\omega)}. \tag{9b}$$

The quantity ϕ defined in (6) is antisymmetric about the center of the layer, i.e. ϕ is an odd function of $c/H - 1/2$. The following approximation to ϕ has the desired antisymmetry and has the correct asymptotic behaviors, (9a) and (9b),

$$\phi = \varepsilon \ln\left(\frac{H-c}{c}\right) + 2\left(\frac{c}{H} - \frac{1}{2}\right)(\phi_H(\alpha, \beta) + \omega(\alpha, \beta)). \tag{10}$$

By comparing (10) with the computed values of ϕ we have found that this approximation is highly accurate. A comparison between the approximation (10) and computed values is shown in Fig. 3, where ϕ is plotted as a function of c/H for several values of α (with $\beta = \alpha/4$). The combination $\phi_H + \omega$ is tabulated in Appendix C.

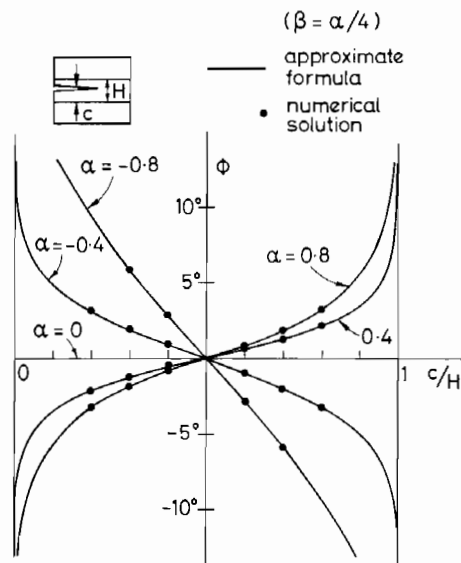Fig. 3. Phase angle $\phi \equiv \tan^{-1}(K_{II}/K_I) - \tan^{-1}(K_{II}^\varepsilon/K_I^\varepsilon)$ for several α values. The full numerical solution is compared with the asymptotic formula, eqn (10). Attention is restricted to $\beta = \alpha/4$.

In summary, the solution to the elasticity problem in Fig. 2 is given by (4) and (6) with c_I and c_{II} tabulated in Appendix C and ϕ given with high accuracy by (10). This solution is now applied to several practical issues in adhesive joint fracture testing.

ELASTIC STRESS SHIELDING FOR A COMPLIANT ADHESIVE

In practice, the fracture energy G_c for adhesive joints is calculated from the measured critical loads by neglecting the presence of the adhesive layer. Provided the layer thickness is small and the crack is long and parallel to the layer, conservation of the J-integral implies that this measure of G_c equals the actual energy released at the crack tip regardless of the crack location (within the adhesive or along the interface). The value of the fracture energy G_c is G_{Ic} for the adhesive if a straight mode I path actually occurs within the adhesive, or is the adhesive/substrate interface fracture energy at the relevant mode of loading if the crack propagates along the interface.

Under remote mode I loading, a crack along the centerline in the layer is locally mode I. If this is a stable crack path and if there is no microstructural change due to the bonding process, the adhesive fractures when the local K_I attains the toughness of the bulk adhesive K_{Ic}. Specialized from (5) by setting $K_{II} = K_{II}^\infty = 0$, the *apparent adhesive toughness* is

$$K_{Ic}^\infty = \left(\frac{1+\alpha}{1-\alpha}\right)^{1/2} K_{Ic} = \left(\frac{\bar{E}_s}{\bar{E}_a}\right)^{1/2} K_{Ic}. \tag{11}$$

An analogous formula was obtained by Wang *et al.* (1978) for the double-cantilever specimen.

In practice, adhesives are usually less rigid than substrates, so that the apparent fracture toughness, measured by the applied stress intensity factor, K_{Ic}^∞, is higher than the toughness of the bulk adhesive, K_{Ic}. Such an effect is due entirely to the elastic mismatch of the two solids and may be referred to as an elastic stress shielding effect. As an example, consider the glass/alumina system. Taking $\alpha = 0.7$, eqn (11) predicts a ratio K_{Ic}^∞/K_{Ic} of 2.4. This is in good agreement with the measured fracture toughness values of Zdaniewski *et al.* (1987).

STABILITY OF CRACK TRAJECTORY UNDER APPLIED MODE I LOADING ($K_{II}^\infty = 0$)

To focus the discussion, assume that the base specimen is subject to a pure mode I loading ($K_{II}^\infty = 0$) so that the centerline of the adhesive layer is a crack trajectory satisfying $K_{II} = 0$. A necessary condition for such centerline trajectories to be observed is that $T < 0$, as already remarked. The behavior of a straight crack displaced away from the centerline suggests another parameter which affects the nature of the crack trajectory. Consider a pre-existing straight crack somewhat off the centerline in the adhesive layer. As illustrated in Fig. 4, if the crack lies above the centerline, it will kink down towards the centerline if $K_{II} > 0$. A formal statement for a crack slightly off a path with $K_{II} = 0$ to kink towards that path is $\partial K_{II}/\partial c > 0$. In other words, a pre-existing crack which is slightly displaced or misaligned will only head towards the centerline (i.e. the path with $K_{II} = 0$) if $\partial K_{II}/\partial c > 0$.
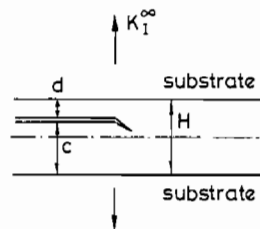

Fig. 4. For $K_{II}^\infty = 0$, a crack above the centerline kinks towards the centerline when $K_{II} > 0$. In general for slightly displaced cracks, the kink will be towards the centerline if $\partial K_{II}/\partial c > 0$.
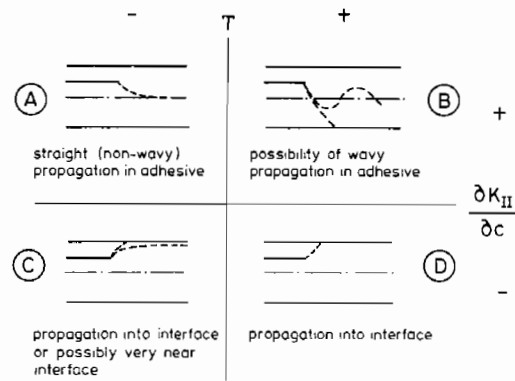
Fig. 5. Conjectured trajectories of crack advance when $K_{II}^\infty = 0$ for a crack displaced slightly off the centerline, depending on the signs of T and $\partial K_{II}/\partial c$.

These considerations suggest that there are four different patterns of fracture behaviors depending on the signs of T and $\partial K_{II}/\partial c$, as illustrated in Fig. 5. We discuss them in turn.

Crack runs stably along the centerline (pattern A)

This is expected when $\partial K_{II}/\partial c > 0$ and $T < 0$. A pre-crack slightly above the centerline will kink towards the centerline because of the positive K_{II}, and the compressive T-stress stabilizes the centerline path.

Crack trajectory is wavy about the centerline (pattern B)

This is expected when $\partial K_{II}/\partial c > 0$ and $T > 0$. Again a pre-crack slightly above the centerline is driven towards the centerline because of the positive K_{II}, but the tensile T-stress destabilizes a crack along the centerline. As a consequence of the two competing effects, the crack trajectory will either be wavy if the positive T is not too large and the positive $\partial K_{II}/\partial c$ can drive the crack back to the centerline, or the crack will diverge towards and join the interface if the positive T is sufficiently large. Quantitative determination of this wavy trajectory has not been performed in this work. To do so would require one to track the wavy path by enforcing the local $K_{II} = 0$. An analysis of this type has been performed by Fleck (1989), where curved trajectories with $K_{II} = 0$ for an array of micro-cracks were determined.

Crack approaches the interface gradually (pattern C)

The negative K_{II} drives a crack away from the centerline, while the compressive T-stress ensures the crack approaches the interface at a small angle. Under remote mode I load, for some material combinations, we find an additional straight path satisfying $K_{II} = 0$ *off* the centerline near one of the interfaces (see Fig. 9).

Crack approaches the interface at a large angle (pattern D)

Figure 5 includes the situation where $\partial K_{II}/\partial c < 0$ and $T > 0$. The crack kinks in an unstable fashion towards the interface.

The sign of $\partial K_{II}/\partial c$ at the centerline can be determined from (6a). It depends only on elastic mismatch constants α and β. Plotted in Fig. 6 is the contour of $\partial K_{II}/\partial c = 0$ on the (α, β) plane. For material combinations with a compliant adhesive layer ($\alpha > 0$, $\beta \approx \alpha/4$), $\partial K_{II}/\partial c$ is positive.

The T-stress is calculated from eqn (4), which when specialized by taking $K_{II}^\infty = 0$ and using (11), gives

$$T = \frac{1-\alpha}{1+\alpha} T^\infty + \sigma^0 + c_1 \frac{K_I^\infty}{\sqrt{H}} \tag{12a}$$

$$T = \frac{1-\alpha}{1+\alpha} T^\infty + \sigma^0 + \left(\frac{1+\alpha}{1-\alpha}\right)^{1/2} c_1 \frac{K_{Ic}}{\sqrt{H}}. \tag{12b}$$
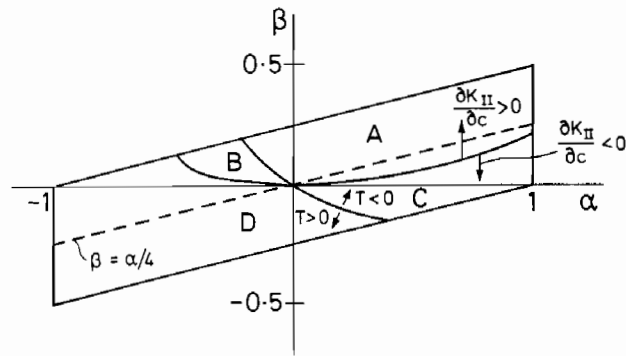
Fig. 6. Regimes of crack path selection for a base specimen subject to mode I loading ($K_{II}^{\infty} = 0$). The contour for $T = 0$ must be shifted if σ^0 and/or T^{∞} are significant.
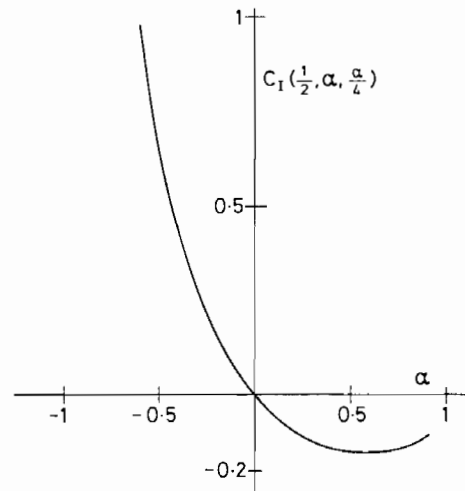

Fig. 7. Coefficient governing contribution to T from K_{I}^{∞} in eqn (12). $c/H = 0.5$, $\beta = \alpha/4$.

Figure 7 presents $c_1(\frac{1}{2}, \alpha, \beta)$ as a function of α (setting $\beta = \alpha/4$), indicating that a negative contribution to the local T-stress is made from the last term in (12) when the layer is compliant. The contour $c_1(\frac{1}{2}, \alpha, \beta) = 0$ is also plotted on Fig. 6. If the contributions of σ^0 and T^{∞} in (12) are negligible, the two contours shown in Fig. 6 divide the (α, β) plane into four regions, labeled as A, B, C, D, corresponding to the four fracture patterns discussed above. The contour for $T = 0$ in Fig. 6 shifts with finite contributions from σ^0 and T^{∞}.

CRACK DEPTH SELECTION WHEN $K_{II}^{\infty} \neq 0$

If the remote loading is somewhat perturbed from mode I, one anticipates that the crack will find a path off the centerline to restore $K_{II} = 0$ locally. This can be addressed rigorously by setting $K_{II} = 0$ and $K_I = K_{Ic}$ in eqn (6), giving

$$K_I^{\infty} = \left(\frac{1+\alpha}{1-\alpha}\right)^{1/2} K_{Ic} \cos \phi, \quad K_{II}^{\infty} = -\left(\frac{1+\alpha}{1-\alpha}\right)^{1/2} K_{Ic} \sin \phi \tag{13}$$

where $\phi(c/H, \alpha, \beta)$ must satisfy

$$\tan \phi = -K_{II}^{\infty}/K_{I}^{\infty}. \tag{14}$$

The location of the crack, c, is obtained from (14) using (10); note that c/H must be such
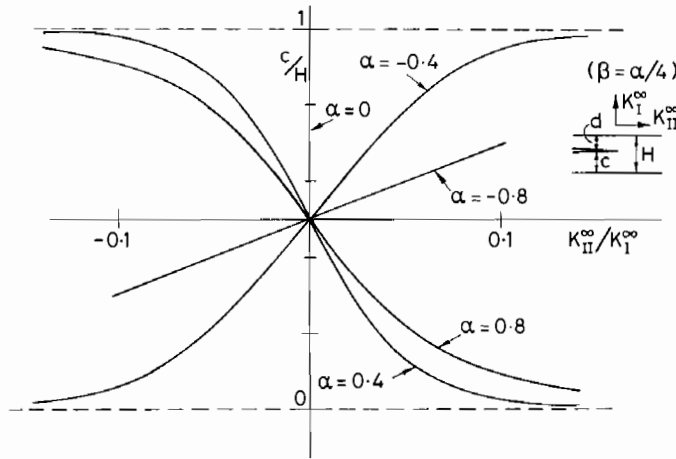
Fig. 8. Crack path selected when K_{II}^∞ is finite. The crack finds a path off the centerline to restore $K_{II} = 0$ locally. For $\alpha < 0$ the crack paths are unstable in the sense $\partial K_{II}/\partial c > 0$ at a fixed K_I^∞, K_{II}^∞

that ϕ is of equal magnitude and opposite sign to the phase angle of the remote loading. The location of the crack as a function of K_{II}^∞/K_I^∞ is shown in Fig. 8 for several α-values (setting $\beta = \alpha/4$). For example, if the remote loading is such that $K_{II}^\infty/K_I^\infty = 0.1$ and $\alpha = 0.8$ ($\beta = 0.2$), the crack with $K_{II} = 0$ is located a distance $c = 0.09\,H$ above the lower interface. The existence of a mode I crack in the layer when $K_{II}^\infty \neq 0$ can only occur if there is a moduli mismatch.

The location of the crack c/H for which $K_{II} = 0$ is given as a function of K_{II}^∞/K_I^∞ in Fig. 9a, for $\alpha = 0.9$ and various β values. A new type of behavior is evident: for β small and positive, such as $\beta = 0.1$, there may exist three locations satisfying $K_{II} = 0$. Consider remote mode I loading, with $\alpha = 0.9$, $\beta = 0.1$. The centerline of the layer satisfies $K_{II} = 0$ but is an unstable path in the sense $\partial K_{II}/\partial c < 0$. Two other locations exist where $K_{II} = 0$; these are close to each interface and are stable in the sense $\partial K_{II}/\partial c > 0$. Cracks paralleling close to an interface have been addressed previously by Hutchinson *et al.* (1987).

The two regimes of (α, β) space for which three crack locations satisfy $K_{II} = 0$ are given in Fig. 9b. The regime in which $\alpha < 0$ and the regime in which $\alpha > 0$ show qualitatively
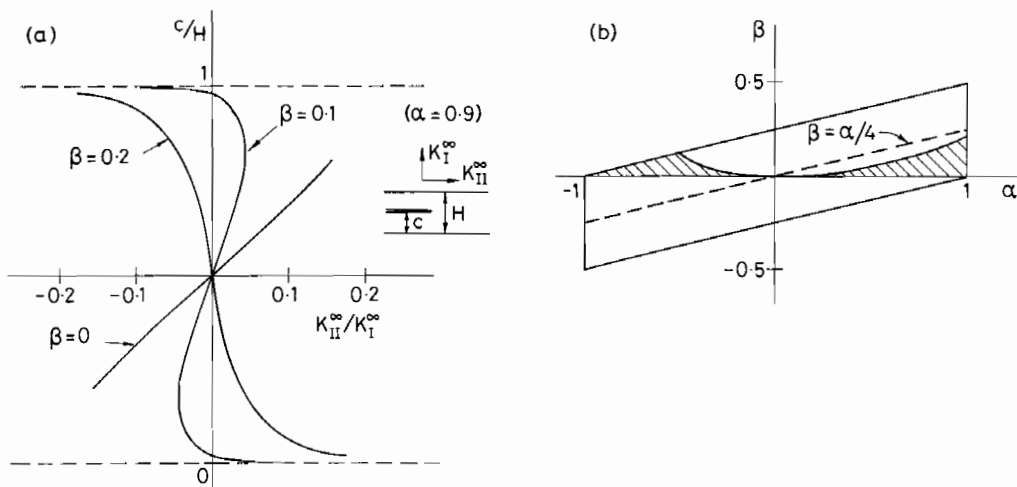
Fig. 9. (a) Location of crack satisfying $K_{II} = 0$ as a function of K_{II}^∞/K_I^∞ for a compliant layer ($\alpha = 0.9$), for various values of β. For β small and positive there can be three locations satisfying $K_{II} = 0$; two of these locations are near the interface and are stable in the sense $\partial K_{II}/\partial c > 0$ at a fixed K_I^∞, K_{II}^∞. (b) The cross hatched region shows the regime of (α, β) for which three crack locations satisfy $K_{II} = 0$.
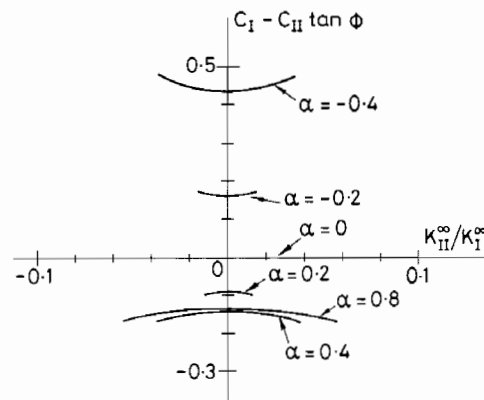
Fig. 10. Coefficient in eqn (15a) for T, for a crack located in the layer with $K_{II} = 0$, $\beta = \alpha/4$.

similar c/H versus $K_{II}^{\infty}/K_{I}^{\infty}$ behaviors. Few practical material combinations lie in either regime.

Next, we examine the T-stress local to the crack tip, for a crack on a straight path with $K_{II} = 0$ and $K_I = K_{Ic}$. The position of the crack path is fixed by the ratio $K_{II}^{\infty}/K_{I}^{\infty}$. Combining (4), (13) and (14), we get

$$T = \frac{1-\alpha}{1+\alpha} T^{\infty} + \sigma^0 + (c_I - c_{II} \tan \phi) \frac{K_I^{\infty}}{\sqrt{H}} \tag{15a}$$

$$T = \frac{1-\alpha}{1+\alpha} T^{\infty} + \sigma^0 + \left(\frac{1+\alpha}{1-\alpha}\right)^{1/2} (c_I \cos \phi - c_{II} \sin \phi) \frac{K_{Ic}}{\sqrt{H}}. \tag{15b}$$

The last contribution in (15a) is plotted in Fig. 10 as a function of $K_{II}^{\infty}/K_{I}^{\infty}$ for various values of the elastic mismatch α. As in the case when $K_{II} = 0$, a straight crack with $K_{II} = 0$ in a compliant layer will have $T < 0$ unless T^{∞} and/or σ^0 are positive and sufficiently large.

CASE STUDIES

Two technically important adhesive systems, epoxy joining metals or ceramics and glass joining ceramics, will be examined in this section using the concepts and numerical results developed above. The relevant mechanical properties used in our discussion are given in Tables 1 and 2. For simplicity, we only consider the situation where the base specimen is under remote mode I loading so that the centerline in the adhesive layer is a pure mode I path ($K_{II} = 0$).

The calculated elastic mismatch constant α is 0.9 for aluminum/epoxy, and 0.7 for alumina/glass, with $\beta \cong \alpha/4$ in each case. Observe that for both cases $\partial K_{II}/\partial c > 0$ (Fig. 6), indicating that a straight crack off the centerline kinks towards the centerline. Whether the crack is stable depends on the sign of the local T-stress.

Focus on the first term in eqn (12). For common base specimens, there is only one

Table 2. Mechanical properties

Material	Thermal expansion coefficient $(MK)^{-1}$	Young's modulus (GPa)	Poisson's ratio
epoxy	70	4	0.34
aluminum	24	71	0.35
glass-7059	5	68	0.24
glass-7570	9	55	0.24
alumina	7	350	0.25

independent applied external load acting on the specimen, implying that T^∞ is linearly connected to K_I^∞, namely

$$T^\infty = gK_I^\infty / \sqrt{a} \tag{16}$$

where g is a dimensionless function of the geometry of the homogeneous base specimen, and a is the crack size. Finite element calculations by Larsson and Carlsson (1973) show that g is somewhere between -0.6 and $+0.2$ for several commonly used homogeneous base specimens. For a typical adhesive joint fracture specimen, the crack size is larger than the adhesive thickness by several orders of magnitude, i.e. $a/H \gg 1$. If the adhesive is more compliant than the substrates, say $\alpha > 0.3$, the first term in (12a) is negligible compared with the third. Hence for systems with compliant adhesives, such as aluminum/epoxy and alumina/glass, it is adequate to consider the competition of the last two terms in (12) only. Note that both are independent of the base specimen geometry, so the conclusions we draw below are independent of specimen type.

The last term in (12) is always negative for compliant adhesive layers; thus the total T-stress is necessarily negative if the residual stress is negative. For alumina/glass-7059, the thermally-induced residual stress in the glass layer is negative; see Zdaniewski et al. (1987). Our theory therefore predicts that the crack will run stably within the glass layer under remote mode I loading (pattern A in Fig. 5). This is observed experimentally by Zdaniewski et al. (1987).

When the residual stress is positive, a numerical estimate is needed to identify which term in (12) is dominant. For the alumina/glass-7570 system, the difference between room temperature and the softening temperature of the glass is 343 K and the residual stress is estimated to be 50 MPa, while the third term in (12) is approximately -37 MPa ($H = 50$ μm is taken). The total T-stress is thus positive. A wavy fracture trajectory (pattern B in Fig. 5b) is therefore expected and was observed in experiments by Zdaniewski et al. (1987).

The residual stress in an epoxy layer joining two ceramics or metals is usually positive due to thermal and/or cure shrinkage. However, our estimates indicate that the magnitude of the residual tensile stress is often less than the third term in (12), resulting in a negative T-stress. This is due to the low Young's modulus of epoxy compared to the substrate materials. For example, if two aluminum substrates are glued together by an epoxy layer of thickness $H = 0.1$ mm at 350 K, the thermal tensile stress is about 15 MPa, but the third term in (12) is -40 MPa. Pattern A in Fig. 5a is anticipated: the crack runs stably within the epoxy layer instead of along the interfaces under predominantly remote mode I loading, as confirmed experimentally by Wang and Suo (1990) and Cao and Evans (1989).

Chai (1987) has observed a wavy crack path in an epoxy layer between aluminum substrates. The crack jumps periodically from one interface to the other across the epoxy layer. The difference in response between the tests performed by Chai and the tests of Wang and Suo (1990) and of Cao and Evans (1989) may be explained in terms of a different sign of the local T-stress. Chai used a heat-setting epoxy of thickness $H = 0.25$ mm; the estimated thermal stress is $\sigma^0 = 60$ MPa while the component of T-stress from the remote loading [the third term in eqn (12a)] is -25 MPa. Hence the total local T-stress is positive in Chai's experiments and the crack is unable to run stably within the epoxy layer. In the work of Wang and Suo and of Cao and Evans the local T-stress is negative and the crack runs stably within the epoxy layer.

Next, we mention some recent fracture tests by Thouless (1990) using double cantilever beam specimens with a model interface consisting of wax/soda lime glass. Thouless observed the crack to run stably along the centerline of the wax layer, in a double cantilever beam sandwich specimen under remote I loading. We expect that the crack will adopt this path, based on the following evaluation of the local T-stress. From values provided by Thouless (1990) and by a private communication, the first term in eqn (12a) is negligible compared to the other two terms, the second term (residual thermal stress) equals 3 MPa and the third term equals -6 MPa. Thus the net T-stress is negative and we predict a stable crack path along the centerline of the wax layer. This result can be contrasted with the double

cantilever specimen of a homogeneous material for which *only* the first term in (12a) is non-zero and positive, leading to the well-known unstable cracking behavior of this specimen.

SUMMARY OF RESULTS

Consider the typical combination of an adhesive layer which is more compliant than the substrates, with $\alpha > 0$, $\beta \approx \alpha/4$. Analysis shows that, provided the residual stress in layer σ^0 is not large and positive, a pre-existing crack in the layer remains trapped in the layer for substantial deviations from pure remote mode I loading. The location of the crack in the layer depends upon the ratio K_{II}^∞/K_I^∞ for any given α and β. If σ^0 is large and tensile, the crack may escape from the layer or may grow along an oscillatory path within the layer.

Now consider a crack in a layer which is stiffer than the substrate, with $\alpha < 0$, $\beta \approx \alpha/4$. A $K_{II} = 0$ path can be found in the layer under remote mixed mode loading. However, the crack will propagate into the interface as $\partial K_{II}/\partial c < 0$, regardless of the sign of T. Unless σ^0 is large and negative, T is positive and the crack is destabilized further.

REFERENCES

Cao, H. C. (1989). Private Communication.
Cao, H. C. and Evans, A. G. (1989). An experimental study of fracture resistance of bimaterial interfaces. *Mech. Mater.* **7**, 295–305.
Chai, H. (1987). A note on crack trajectory in an elastic strip bounded by rigid substrates. *Int. J. Fract.* **32**, 211–213.
Coker, E. G. and Filon, L. G. N. (1931). *Treatise on Photoelastisity*, p. 136. Cambridge University Press, U.K.
Cotterell, B. and Rice, J. R. (1980). Slightly curved or kinked cracks. *Int. J. Fract.* **16**, 155–169.
Dundurs, J. (1969). Discussion of a paper by D. B. Bogy. *J. Appl. Mech.* **36**, 650–652.
Erdogan, F. and Gupta, G. D. (1971) The stress analysis of multi-layered composites with a flaw. *Int. J. Solids Structures* **7**, 39–61.
Fleck, N. A. (1989). Brittle fracture due to an array of microcracks. Harvard University Report MECH-148.
Larsson, S. G. and Carlsson, A. J. (1973). Influence of non-singular stress terms and specimen geometry on small-scale yielding at crack tips in elastic–plastic materials. *J. Mech. Phys. Solids* **21**, 263–277.
Hutchinson, J. W., Mear, M. E. and Rice, J. R. (1987). Crack paralleling an interface between dissimilar materials. *J. Appl. Mech.* **54**, 828–832.
Suga, T., Elssner, G. and Schmander, S. (1988). Composite parameters and mechanical compatibility of material joints. *J. Composite Mater.* **22**, 917–934.
Suo, Z. and Hutchinson, J. W. (1989). Sandwich specimens for measuring interface crack toughness. *J. Mater. Sci. Engng* **A107**, 135–143.
Tada, H., Paris, P. C. and Irwin, G. R. (1985). *Stress Analysis of Cracks Handbook.* Del Research, St Louis, MO.
Thouless, M. D. (1990). Fracture of a model interface under mixed-mode loading. *Acta Metall. Mater.* **38**, 1135–1140.
Wang, J.-S. and Suo, Z. (1990). Experimental determination of interfacial toughness curves using brazil nut sandwiches. *Acta Metall. Mater.* **38**, 1279–1290.
Wang, S. S., Mandell, J. F. and McGarry, F. J. (1978). An analysis of the crack tip stress field in DCB adhesive fracture specimens. *Int. J. Fracture* **14**, 39–58.
Zdaniewski, W. A., Conway, J. C., Jr and Kirchner, H. P. (1987). Effect of joint thickness and residual stresses on the properties of ceramic adhesive joints: II, Experimental results. *J. Am. Ceram. Soc.* **70**, 110–118.

APPENDIX A: INTEGRAL EQUATION FORMULATION AND SOLUTION

In this Appendix, we set up and solve the integral equation for the plane elasticity problem specified in Fig. 2.

A.1. *Formulation of integral equation*

A layer of material 2 is sandwiched in an infinite medium of material 1. Each material is taken to be isotropic and linear elastic. A semi-infinite crack lies a distance c above the lower interface, in the adhesive layer. The thickness H of the layer is taken to be unity since the H dependence of the solution is known. A Cartesian coordinate system is centered on the crack tip, with the x_1 axis coincident with the crack.

We prescribe loading in the far field as the standard crack tip field of a crack in a homogeneous body, characterized by the remote stress intensity factors K_I^∞ and K_{II}^∞. [The next higher order term T^∞ is explicitly incorporated in the solution (12b) already.] The asymptotic problem of the cracked adhesive layer is solved in terms of K_I^c and K_{II}^c by the method of distributed dislocations. The crack is modeled by a distribution of dislocations such that the tractions on the crack line vanish. Plane strain deformations are assumed; for plane stress, replace ν by $\nu/(1+\nu)$.

Let $b_i(\xi)$ be the x_i component of an edge dislocation located on the crack line at $x_1 = \xi$, $x_2 = 0$. The stresses at point $x_1 = x$, $x_2 = 0$ on the crack line induced by the dislocation are given by

$$\sigma_{i2}(x) = \frac{\mu_2}{4\pi(1-v_2)}\left(2\frac{b_i(\xi)}{x-\xi} + f_{ij}(x-\xi)b_j(\xi)\right) \tag{A1}$$

where the repeated suffix j, here and elsewhere, refers to a sum over $j = 1, 2$. The kernels $f_{ij}(x-\xi)$ are constructed in Appendix B. They are well behaved in the whole range $-\infty < \xi < \infty$, with asymptotes

$$f_{ij}(\zeta) = O\left(\frac{1}{\zeta}\right) \quad \text{as} \quad |\zeta| \to \infty. \tag{A2}$$

A semi-infinite crack is represented by a distribution of dislocations lying along the negative x_1 axis, such that the tractions vanish for $x_1 < 0$. Thus, the distribution $b_i(\xi)$ for $\xi < 0$ is governed by

$$\int_{-\infty}^{0} \frac{2b_i(\xi)}{x-\xi} + f_{ij}(x-\xi)b_j(\xi)\,\mathrm{d}\xi = 0, \quad x < 0, \quad i = 1,2 \tag{A3}$$

where the first integral is the Cauchy Principal Value integral.

The crack face displacements δ_i are related to the dislocation distribution by

$$\delta_i(x) = \int_{x}^{0} b_i(\xi)\,\mathrm{d}\xi, \quad x < 0, \quad i = 1, 2. \tag{A4}$$

The form of $b_i(\xi)$ must be such that the crack displacements approach the remote field specified by K^∞ as $\xi \to \infty$, and must be consistent with the near-tip field with unknown intensity K as $\xi \to 0$. Thus,

$$b_i(\xi) \sim \frac{2}{\sqrt{-2\pi\xi}}\frac{(1-v_1)}{\mu_1}K_i^\infty \quad \text{as} \quad \xi \to -\infty \tag{A5}$$

and

$$b_i(\xi) \sim \frac{2}{\sqrt{-2\pi\xi}}\frac{(1-v_2)}{\mu_2}K_i \quad \text{as} \quad \xi \to 0 \tag{A6}$$

where K_1 denotes the mode II stress intensity factor K_{II}, and K_2 denotes the mode I stress intensity factor K_I.

In order to reduce the range of the integral equation to a finite interval, we make the changes of variables

$$x = \frac{u-1}{u+1}, \quad -1 < u < 1$$

$$\xi = \frac{t-1}{t+1}, \quad -1 < t < 1 \tag{A7}$$

which gives

$$\zeta = x - \xi = \frac{2(u-t)}{(u+1)(t+1)}. \tag{A8}$$

Then, with $c_i(t) \equiv b_i(\xi)$, the linear system of two integral equations becomes

$$\int_{-1}^{1} \frac{(u+1)}{(u-t)(t+1)}c_i(t)\,\mathrm{d}t + \int_{-1}^{1} f_{ij}(\zeta)c_i(t)\frac{\mathrm{d}t}{(1+t)^2} = 0, \quad |u| < 1 \tag{A9}$$

where $\oint$ denotes the Cauchy Principal Value integral.

Based on the asymptotic behavior of $b_i(\xi)$ as $\xi \to 0$ and $\xi \to -\infty$, a complete representation for $c_i(t)$ is

$$c_i(t) = \left(\frac{1+t}{1-t}\right)^{1/2}\sum_{k=0}^{\infty}a_{ik}T_k(t), \quad i = 1, 2 \tag{A10}$$

where $T_k(t)$ is the Chebyshev polynomial of the first kind of degree k and a_{ik} are a doubly infinite set of real coefficients which must be determined by the solution process.

From the asymptotic behavior of $b_i(\xi)$, eqns (A5) and (A6), the remote stress intensity factors K_i^∞ and the crack tip stress intensity factors K_i may be expressed in terms of a_{ik},

$$K_i^\infty = \left(\frac{\pi}{2}\right)^{1/2}\frac{\mu_2}{(1-v_2)}\left(\frac{1+\alpha}{1-\alpha}\right)\sum_{k=0}^{\infty}(-1)^k a_{ik} \tag{A11}$$

and

$$K_i = \left(\frac{\pi}{2}\right)^{1/2} \frac{\mu_2}{(1-\nu_2)} \sum_{k=0}^{\infty} a_{ik} \tag{A12}$$

where α is defined in eqn (3).

Equation (A11) represents two equations for the as in terms of the specified K^∞s, and (A12) are the two equations for evaluating the Ks.

A.2. *Solution of integral equation*

When the representation for $c_i(t) \equiv b_i(\xi)$, eqn (A10) is substituted into the integral eqn (A9), the first term of (A9) maybe integrated exactly to give

$$\int_{-1}^{1} \frac{(u+1)}{(u-t)(t+1)} c_i(t)\, dt = -\pi(1+u) \sum_{k=1}^{\infty} a_{ik} U_{k-1}(u) \tag{A13}$$

where $U_k(u)$ is the Chebyshev polynomial of the second kind of degree k.

The factor of $(1+t)^2$ in the second term of eqn (A9) presents a problem in evaluation of the integral near $t = -1$. Recalling the asymptotic behavior for $f_{ij}(\zeta)$, eqn (A2), we proceed by introducing a function $F_{ij}(\zeta)$ in order to extract a factor of $(t+1)$ from $f_{ij}(\zeta)$:

$$F_{ij}(\zeta) = f_{ij}(\zeta)\sqrt{\zeta^2+4} = \frac{f_{ij}(\zeta)}{(t+1)} \frac{1}{p(t,u)} \tag{A14}$$

where

$$p(t,u) \equiv \frac{u+1}{2} [(u+1)^2(t+1)^2 + (u-t)^2]^{-1/2}.$$

The function $p(t,u)$ is well behaved for $|t| \leqslant 1$, $|u| \leqslant 1$.

Substitution of (A14) and (A10) into the second term of (A9) then gives

$$\int_{-1}^{1} f_{ij}(\zeta)c_j(t) \frac{dt}{(1+t)^2} \sum_{k=0}^{\infty} I_{ijk}(u)a_{jk}, \quad |u| < 1 \tag{A15}$$

where

$$I_{ijk}(u) = \int_{-1}^{1} \frac{p(t,u)}{\sqrt{1-t^2}} F_{ij}(\zeta)T_k(t)\, dt. \tag{A16}$$

Equation (A16) can be integrated numerically without further problems. However, to reduce computer time we express the functions $F_{ij}(\zeta)$ by a Chebyshev series approximation. Noting that $f_{ij}(\zeta)$ and $F_{ij}(\zeta)$ are either odd or even in ζ, we write

$$F_{ij}(\zeta) = \sum_{k=1}^{M} d_{ijk}T_{k-1}(s) - \tfrac{1}{2}d_{ij1}, \quad \zeta = \frac{s-1}{s+1} \tag{A17}$$

where s ranges from -1 to 1, as ζ varies from $-\infty$ to 0. The coefficients d_{ijk} are found from the known kernel functions $F_{ij}(\zeta)$, and the number of terms M is usually taken to be $M = 40$.

We can now rewrite the integral equation (A9) as a linear system of equations in a_{ij}, via eqns (A13) and (A15):

$$(1+u) \sum_{k=1}^{N} a_{ik}U_{k-1}(u) + \sum_{k=0}^{N} I_{ijk}(u)a_{jk} = 0, \quad |u| < 1, \quad i = 1,2 \tag{A18}$$

where the infinite sums have been replaced by a finite sum in $N+1$ terms.

The truncated form of (A11) provides the additional equations

$$\sum_{k=0}^{N} (-1)^k a_{ik} = \left(\frac{2}{\pi}\right)^{1/2} \frac{(1-\nu_2)}{\mu_2} \left(\frac{1-\alpha}{1+\alpha}\right) K_i^\infty. \tag{A19}$$

We solve for the $2(N+1)$ unknowns a_{ik} $(i = 1,2; k = 0,\ldots,N)$ by satisfying (A18) at N Gauss–Legendre points for u in the interval $-1 < u < 1$, and also by satisfying (A19). A convergence study showed that an accuracy of 0.1% is achievable for $N = 20$. Once the coefficients a_{ij} have been found for any remote loading K^∞, geometry c/H and elastic constants α, β, the local stress intensity factors at the crack tip in the adhesive layer are computed from eqn (A12). The formula for the energy release rate, (5), forms a consistency check and provides a measure of the accuracy of the solution procedure.

A.3. *Evaluation of the T-stress*

The stress $\sigma_{11}(x)$ at point $x_1 = x$, $x_2 = 0$ on the crack line induced by a dislocation $b_i(x_1 = \xi)$ is obtained from the dislocation solution given in Appendix **B**:

$$\sigma_{11}(x) = \frac{\mu_2}{4\pi(1-\nu_2)}\left(\frac{2b_2(\xi)}{x-\xi} + g_i(x-\xi)b_i(\xi)\right) \tag{A20}$$

where we continue with the summation convention for a repeated suffix i over 1 and 2. The non-singular kernel $g_i(x-\xi)$ is given in Appendix B.

When we represent the semi-infinite crack under a remote K^∞ field by a distribution of dislocations along the negative x_1 axis, the stress $\sigma_{11}(x)$ induced by the dislocations is

$$\sigma_{11}(x) = \frac{\mu_2}{4\pi(1-\nu_2)}\int_{-\infty}^0 \frac{2b_2(\xi)}{x-\xi} + g_i(x-\xi)b_i(\xi)\,\mathrm{d}\xi \tag{A21}$$

where the first integral is the Cauchy Principal Value integral.

Using the change of variables (A7) and (A8), and the representation $c_i(t) \equiv b_i(\xi)$ given by (A10), the Cauchy part of (A21) may be integrated analytically for $x < 0$ to give

$$\int_{-\infty}^0 \frac{2b_2(\xi)}{x-\xi}\,\mathrm{d}\xi = -2\pi\sum_{k=1}^\infty a_{2k}(1+u)U_{k-1}(u), \quad -1 < u < 1. \tag{A22}$$

In the limit $x \to 0^-$, $u \to 1$, $\sigma_{11}(x)$ equals T and eqn (A22) reduces to

$$\int_{-\infty}^0 \frac{2b_2(\xi)}{x-\xi}\,\mathrm{d}\xi = -4\pi\sum_{k=0}^\infty k\,a_{2k}, \quad x \to 0^-. \tag{A23}$$

Now consider the second term on the right-hand side of eqn (A21). With the change of variable $\xi \to t$ specified by eqn (A7), ζ given by eqn (A8) and $c_i(t) \equiv b_i(\xi)$, we derive

$$I(x) \equiv \int_{-\infty}^0 g_i(x-\xi)b_i(\xi)\,\mathrm{d}\xi = \int_{-1}^1 g_i(\zeta)c_i(t)\frac{\mathrm{d}t}{(1+t)^2}. \tag{A24}$$

In the limit $x \to 0^-$, the above integral $I(0^-)$ exists and provides a further contribution to the T-stress. In this limit $\zeta = -\xi$ and $(1+t) = 2/(1+\zeta)$. The troublesome $(1+t)^2$ factor in the denominator of the right-hand side of eqn (A24) is removed by using representation (A10) for $c_i(t)$ and by separating out a factor $(1+t)$ from $g_i(\zeta)$:

$$g_i(\zeta) \equiv h_i(\zeta)\left(\frac{1+t}{2}\right) = \frac{h_i(\zeta)}{1+\zeta}. \tag{A25}$$

The well-behaved function $h_i(\zeta)$, defined via (A25), is represented by a Chebyshev-series approximation in M terms:

$$h_i(\zeta) = \sum_{k=1}^M d_{ik}T_{k-1}(t) - \tfrac{1}{2}d_{i1}, \quad -\zeta = \frac{t-1}{t+1}. \tag{A26}$$

The coefficients d_{ik} are found from the known kernel functions $h_i(\zeta)$, and M is usually taken to be $M = 40$.

A particularly simple expression for the integral $I(0^-)$ in (A24) is now obtained by substituting eqns (A10), (A25) and (A26) into (A24), and by integrating analytically

$$I(0^-) = \frac{\pi}{2}\sum_{k=1}^{N,M} a_{ik}d_{ik} \tag{A27}$$

where the upper limit of the sum is taken to be the smaller of terms N used in the representation for $c_i(t)$, and the number of terms M used in the representation for $h_i(\zeta)$. As elsewhere, the repeated suffix i denotes a sum over $i = 1, 2$.

The T-stress is given by substituting eqns (A23) and (A27) into eqn (A20):

$$T = \sigma_{11}(x = 0^-) = \frac{\mu_2}{(1-\nu_2)}\left(-\sum_{k=0}^N k\,a_{2k} + \frac{1}{8}\sum_{k=1}^{N,M}\sum_{i=1}^2 a_{ik}d_{ik}\right). \tag{A28}$$

Tabulated values for T are given in Appendix C, where representation (4) is used for T.

APPENDIX B: A DISLOCATION IN THE ADHESIVE LAYER

The dislocation solution used as the kernel in the integral eqn (A1) and in the expression for the T-stress, eqn (A20), is summarized here.
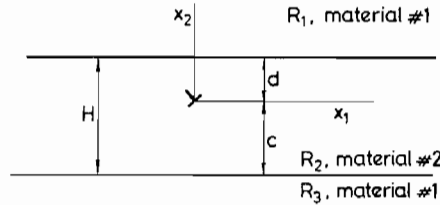
Fig. B1. Edge dislocation in adhesive layer.

The plane elasticity problem is specified in Fig. B1. An edge dislocation with components b_1 and b_2 lies at the origin a distance c above the lower interface of the bonded sandwich structure. This dislocation lies a distance d below the upper interface, and the thickness of the layer is $H = c+d$. The solution is obtained by superimposing the solutions to two problems:

(1) An isolated dislocation at the origin in a full plane, made from material 2. The material in the half-plane $x_2 > d$ and in the half-plane $x_2 < -c$ is then allowed to transform from material 2 to material 1. We shall allow the transformation to occur in a manner which generates a displacement mismatch $\Delta\mathbf{u}(\mathbf{x})$ at $y = d$ and $y = -c$, but does not alter the stresses anywhere.
(2) A strip of material 2 of thickness $H = c+d$, sandwiched between two half-planes of material 1, with a displacement mismatch of $-\Delta\mathbf{u}(\mathbf{x})$ from Problem 1 at the boundaries between the two materials.

Problem 1

The solution to an isolated dislocation at the origin in a full plane made from material 2 is given compactly by the Muskhelishvili potentials

$$\phi = A \ln z, \quad \Omega = \bar{A} \ln z \tag{B1}$$

where

$$z \equiv x_1 + ix_2, \quad A \equiv \frac{\mu_2}{4\pi(1-\nu_2)}(b_2 - ib_1), \quad \sigma_{11} + \sigma_{22} = 2(\phi'(z) + \overline{\phi'(z)})$$

$$\sigma_{22} - \sigma_{11} + i2\sigma_{12} = 2[(\bar{z}-z)\phi''(z) + \Omega'(z) + \phi'(z)] \tag{B2}$$

and the displacements u_1, u_2 are given for plane strain by

$$2\mu_2(u_1 + iu_2) = (3 - 4\nu_2)\phi(z) + (\bar{z}-z)\overline{\phi'(z)} - \overline{\Omega(z)}. \tag{B3}$$

The stresses at $(\zeta, 0)$ induced by the dislocation are

$$\sigma_{i2}(\zeta) = \frac{\mu_2}{4\pi(1-\nu_2)} \frac{2b_i}{\zeta}, \quad \sigma_{11}(\zeta) = \frac{\mu_2}{4\pi(1-\nu_2)} \frac{2b_2}{\zeta}. \tag{B4}$$

We now let material 2 transform to material 1 for $x_2 > d$ and $x_2 < -c$, but keep the Muskhelishvili potentials fixed. The stresses given by (B3) and (B4) remain unaltered but displacements change in region R_1 where $x_2 > d$, and in region R_2 where $x_2 < -c$. Define the displacement jump at these boundaries $\Delta\mathbf{u}$ by

$$\Delta\mathbf{u} = \mathbf{u}_{①} - \mathbf{u}_{②}$$

where ① refers to material 1 and ② refers to material 2. The jump in displacement gradient

$$\frac{\partial \Delta u_1}{\partial x_1} + i\frac{\partial \Delta u_2}{\partial x_1}$$

is derived from (B3) as

$$\frac{2\mu_2}{4(1-\nu_2)}\left(\frac{\partial \Delta u_1}{\partial x_1} + i\frac{\partial \Delta u_2}{\partial x_1}\right) = -\left(\frac{\alpha+\beta}{1+\alpha}\right)\phi'(z) - \left(\frac{\alpha-\beta}{1+\alpha}\right)[(\bar{z}-z)\overline{\phi''(z)} - \overline{\Omega'(z)}] \tag{B5}$$

which upon substitution for ϕ, Ω from (B1) and separation of real and imaginary parts gives

$$\frac{\partial \Delta u_1}{\partial x_1} = \frac{b_1}{\pi(1+\alpha)}\left[(2\alpha-\beta)\frac{x_2}{r^2} - 2(\alpha-\beta)\frac{x_2^3}{r^4}\right] + \frac{b_2}{\pi(1+\alpha)}\left[-\beta\frac{x_1}{r^2} + 2(\alpha-\beta)\frac{x_1 x_2^2}{r^4}\right]$$

$$\frac{\partial \Delta u_2}{\partial x_1} = \frac{b_1}{\pi(1+\alpha)}\left[\beta\frac{x_1}{r^2} + 2(\alpha-\beta)\frac{x_1 x_2^2}{r^4}\right] + \frac{b_2}{\pi(1+\alpha)}\left[\beta\frac{x_2}{r^2} + 2(\alpha-\beta)\frac{x_2^3}{r^4}\right]$$

$$\tag{B6}$$

where $r^2 \equiv x_1^2 + x_2^2$.

We superpose the solution to Problem 2 in order to cancel the displacement gradient mismatch given by (B6).

Problem 2. Dislocation-free strip problem

Consider a dislocation-free strip of thickness H made from material 2, sandwiched between two half-planes of material 1. A displacement gradient jump of equal magnitude and opposite sign to that specified by (B6) is applied on $x_2 = d$ and $x_2 = -c$. This displacement mismatch gives rise to stresses which are bounded everywhere. Such a multilayer problem is solved conveniently using Fourier transforms with two real potentials $U(x_1, x_2)$ and $X(x_1, x_2)$; see Coker and Filon (1931). These potentials satisfy

$$\nabla^4 U = 0, \quad \nabla^2 X = 0, \quad \frac{\partial^2 X}{\partial x_1 \, \partial x_2} = \tfrac{1}{4}\nabla^2 U. \tag{B7}$$

The stresses and displacements can be derived from

$$\sigma_{11} = \frac{\partial^2 U}{\partial x_2^2}, \quad \sigma_{22} = \frac{\partial^2 U}{\partial x_1^2}, \quad \sigma_{12} = -\frac{\partial^2 U}{\partial x_1 \, \partial x_2}$$

$$2\mu u_1 = -\frac{\partial U}{\partial x_2} + 4(1-\nu)\frac{\partial X}{\partial x_2}, \quad 2\mu u_2 = -\frac{\partial U}{\partial x_2} + 4(1-\nu)\frac{\partial X}{\partial x_1}. \tag{B8}$$

The general approach to the multilayer problem is as follows. For each layer, the solution of $U(x, y)$ and $X(x, y)$ can be separated into two parts: one is symmetric in changing x to $-x$, and the other is antisymmetric. A dislocation of strength b_1 in Problem 1 induces a field in Problem 2 which can be represented by a symmetric U, termed $U^s(x_1, x_2)$ and an antisymmetric X, termed $X^a(x_1, x_2)$. Conversely, a dislocation of strength b_2 gives rise to an antisymmetric U, which we denote by $U^a(x, y)$ and a symmetric X, which we denote by $X^s(x, y)$. We shall consider the solution associated with b_1 and b_2 in turn.

b_1 *solution.* The potentials $U^s(x, y)$ and $X^a(x, y)$, upon satisfying (B7), can be represented by Fourier integrals

$$U^s(x, y) = b_1 \int_0^\infty \left[\left(\frac{A_1}{\lambda^2} + \frac{A_2}{\lambda} y\right) e^{-\lambda y} + \left(\frac{A_3}{\lambda^2} + \frac{A_4}{\lambda} y\right) e^{\lambda y} \right] \cos \lambda x \, d\lambda$$

$$X^a(x, y) = b_1 \int_0^\infty \frac{1}{2\lambda^2}[A_2 \, e^{-\lambda y} + A_4 \, e^{\lambda y}] \sin \lambda x \, d\lambda \tag{B9}$$

where the four coefficients A_i are functions of λ.

Potentials $U^s(x, y)$ and $X^a(x, y)$ exist for each of the three layers R_1, R_2 and R_3 shown in Fig. B1. The Fourier coefficients A_i are designated C_i in R_1, D_i in R_2 and E_i in R_3. Since U^s and X^a remain bounded as $x_2 \to \infty$ in R_1, $C_3 = C_4 = 0$ by eqn (B9). Similarly, $E_1 = E_2 = 0$ in R_3. The stresses and displacements in each layer are given by eqns (B8).

The problem is to determine the coefficients D_i in the strip R_2, and thence the stresses in R_2, from the known displacement gradient mismatch at $x_2 = d$, and $x_2 = -c$ given by the b_1 solution in (B6). To proceed, we take the appropriate Fourier transforms $\Delta \tilde{u}_{1,1}$ and $\Delta \tilde{u}_{2,1}$ of the displacement gradient mismatch $\partial \Delta u_1 / \partial x_1$ and $\partial \Delta u_2 / \partial x_1$, respectively:

$$\Delta \tilde{u}_{1,1}(\lambda, x_2) = \frac{2}{\pi}\int_0^\infty \frac{\partial \Delta u_1}{\partial x_1} \cos \lambda x \, dx$$

$$\Delta \tilde{u}_{2,1}(\lambda, x_2) = \frac{2}{\pi}\int_0^\infty \frac{\partial \Delta u_2}{\partial x_1} \sin \lambda x \, dx. \tag{B10}$$

Substitution of the b_1 part of (B6) into (B10) and evaluation of the integrals gives

$$\left. \begin{aligned}
\Delta \tilde{u}_{1,1}(\lambda, d) &= \frac{b_1}{\pi}\left(\frac{\alpha(1-\lambda d) + \beta\lambda d}{(1+\alpha)}\right) e^{-\lambda d} \\[4pt]
\Delta \tilde{u}_{2,1}(\lambda, d) &= \frac{b_1}{\pi}\left(\frac{\beta(1-\lambda d) + \alpha\lambda d}{(1+\alpha)}\right) e^{-\lambda d} \\[4pt]
\Delta \tilde{u}_{1,1}(\lambda, -c) &= -\frac{b_1}{\pi}\left(\frac{\alpha(1-\lambda c) + \beta\lambda c}{(1+\alpha)}\right) e^{-\lambda c} \\[4pt]
\Delta \tilde{u}_{2,1}(\lambda, -c) &= \frac{b_1}{\pi}\left(\frac{\beta(1-\lambda c) + \alpha\lambda c}{(1+\alpha)}\right) e^{-\lambda c}
\end{aligned} \right\}. \tag{B11}$$

We determine D_i by matching tractions and displacement gradients at the strip boundaries $x_2 = d$ and $x_2 = -c$, in the transformed variable λ. Hence, in matrix form,

$$\mathbf{M}_1\mathbf{D} + \mathbf{M}_2\mathbf{E} = \mathbf{v}_1$$

$$\mathbf{M}_3\mathbf{D} + \mathbf{M}_4\mathbf{C} = \mathbf{v}_2 \tag{B12}$$

where

$$\mathbf{M}_1 = \mathrm{e}^{-\lambda d} \begin{bmatrix} -1 & \lambda c & -\mathrm{e}^{-2\lambda c} & \lambda c\,\mathrm{e}^{-2\lambda c} \\ -1 & (1+\lambda c) & \mathrm{e}^{-2\lambda c} & (1-\lambda c)\,\mathrm{e}^{-2\lambda c} \\ 0 & \Sigma/2 & 0 & -\dfrac{\Sigma}{2}\mathrm{e}^{-2\lambda c} \\[2ex] 0 & \Sigma/2 & 0 & \dfrac{\Sigma}{2}\mathrm{e}^{-2\lambda c} \end{bmatrix}$$

$$\mathbf{M}_2 = \mathrm{e}^{-\lambda(H+c)} \begin{bmatrix} 1 & -\lambda c \\ -1 & (\lambda c-1) \\ -\left(\dfrac{\alpha-\beta}{1-\alpha}\right) & \left(\dfrac{\alpha-\beta}{1-\alpha}\right)\lambda c+\tfrac{1}{2} \\[2ex] -\left(\dfrac{\alpha-\beta}{1-\alpha}\right) & -\left(\dfrac{\alpha-\beta}{1-\alpha}\right)(1-\lambda c)-\tfrac{1}{2} \end{bmatrix}$$

$$\mathbf{M}_3 = \mathrm{e}^{-\lambda c} \begin{bmatrix} -\mathrm{e}^{-2\lambda d} & -\lambda d\,\mathrm{e}^{-2\lambda d} & -1 & -\lambda d \\ -\mathrm{e}^{-2\lambda d} & (1-\lambda d)\,\mathrm{e}^{-2\lambda d} & 1 & (1+\lambda d) \\ -\left(\dfrac{\alpha-\beta}{1-\alpha}\right)\mathrm{e}^{-2\lambda d} & \left(-\left(\dfrac{\alpha-\beta}{1-\alpha}\right)\lambda d+\dfrac{\Sigma}{2}\right)\mathrm{e}^{-2\lambda d} & -\left(\dfrac{\alpha-\beta}{1-\alpha}\right) & -\left(\dfrac{\alpha-\beta}{1-\alpha}\right)\lambda d-\dfrac{\Sigma}{2} \\[2ex] \left(\dfrac{\alpha-\beta}{1-\alpha}\right)\mathrm{e}^{-2\lambda d} & \left(\left(\dfrac{\alpha-\beta}{1-\alpha}\right)(\lambda d-1)+\dfrac{\Sigma}{2}\right)\mathrm{e}^{-2\lambda d} & -\left(\dfrac{\alpha-\beta}{1-\alpha}\right) & -\left(\dfrac{\alpha-\beta}{1-\alpha}\right)(\lambda d+1)+\dfrac{\Sigma}{2} \end{bmatrix}$$

$$\mathbf{M}_4 = \mathrm{e}^{-\lambda(H+d)} \begin{bmatrix} 1 & \lambda d \\ 1 & \lambda d-1 \\ 0 & -\tfrac{1}{2} \\ 0 & -\tfrac{1}{2} \end{bmatrix}$$

$$\Sigma \equiv \frac{1+\alpha}{1-\alpha}, \quad \mathbf{C} = \begin{pmatrix} C_1 \\ C_2 \end{pmatrix}, \quad \mathbf{D} = \begin{bmatrix} D_1 \\ D_2 \\ D_3 \\ D_4 \end{bmatrix}, \quad \mathbf{E} = \begin{pmatrix} E_3 \\ E_4 \end{pmatrix}$$

$$\mathbf{v}_1 = -\frac{\mu_2\Sigma}{2(1-\nu_2)} \frac{\mathrm{e}^{-\lambda(H+c)}}{b_1} \begin{bmatrix} 0 \\ 0 \\ \Delta\tilde{u}_{1,1}(\lambda,-c) \\ \Delta\tilde{u}_{2,1}(\lambda,-c) \end{bmatrix}, \quad \mathbf{v}_2 = -\frac{\mu_2\Sigma}{2(1-\nu_2)} \frac{\mathrm{e}^{-\lambda(H+d)}}{b_1} \begin{bmatrix} 0 \\ 0 \\ \Delta\tilde{u}_{1,1}(\lambda,d) \\ \Delta\tilde{u}_{2,1}(\lambda,d) \end{bmatrix}.$$

Equations (B12) can be combined to a single matrix equation

$$\begin{pmatrix} \mathbf{M}_1 & \mathbf{M}_2 & \mathbf{0} \\ \mathbf{M}_3 & \mathbf{0} & \mathbf{M}_4 \end{pmatrix} \begin{pmatrix} \mathbf{D} \\ \mathbf{E} \\ \mathbf{C} \end{pmatrix} = \begin{pmatrix} \mathbf{v}_1 \\ \mathbf{v}_2 \end{pmatrix} \tag{B13}$$

which is solved by Gaussian elimination in order to determine $\mathbf{D}$.

b_2 *solution.* In similar manner, we can solve for the stresses and displacements in a strip of material 2 sandwiched between two half-planes of material 1, due to displacement mismatches on $x_2 = d$ and $x_2 = -c$. The displacement mismatch is $-\Delta\mathbf{u}(\mathbf{x})$ where $\Delta\mathbf{u}$ is the displacement mismatch due to a dislocation of strength b_2 in Problem 1, specified by eqn (B6). The stresses and displacements are derived from $U^\mathrm{a}(x,y)$ and $X^\mathrm{s}(x,y)$ which, upon satisfying (B7), can be represented by the Fourier integral

$$U^\mathrm{a}(x,y) = b_2 \int_0^\infty \left[\left(\frac{B_1}{\lambda^2} + \frac{B_2}{\lambda} y \right) \mathrm{e}^{-\lambda y} + \left(\frac{B_3}{\lambda^2} + \frac{B_4}{\lambda} y \right) \mathrm{e}^{\lambda y} \right] \sin \lambda x \, \mathrm{d}x$$

$$X^\mathrm{s}(x,y) = -b_2 \int_0^\infty \frac{1}{2\lambda^2} \left[B_2\,\mathrm{e}^{-\lambda y} + B_4\,\mathrm{e}^{\lambda y} \right] \cos \lambda x \, \mathrm{d}\lambda \tag{B14}$$

where the four coefficients B_i, like the coefficients A_i, are functions of λ. We designate the Fourier coefficients B_i by F_i in R_1, G_i in R_2 and H_i in R_3. The stresses and displacements in each layer are given by (B8) as before.

The problem is to determine the coefficients G_i in the strip R_2 from the known displacement gradient mismatch at $x_2 = d$ and $x_2 = -c$, given by the b_2 solution in (B6). To proceed, we take the Fourier transforms $\Delta\tilde{u}_{1,1}$ and $\Delta\tilde{u}_{2,1}$:

$$\Delta \tilde{u}_{1,1}(\lambda, x_2) = \frac{2}{\pi} \int_0^\infty \frac{\partial \Delta u_1}{\partial x_1} \sin \lambda x \, dx$$

$$\Delta \tilde{u}_{2,1}(\lambda, x_2) = \frac{2}{\pi} \int_0^\infty \frac{\partial \Delta u_2}{\partial x_1} \cos \lambda x \, dx. \tag{B15}$$

We now substitute the b_2 part of (B6) into (B15) and evaluate the integrals, giving

$$\left.\begin{aligned}
\Delta \tilde{u}_{1,1}(\lambda, d) &= \frac{b_2}{\pi} \left(\frac{-\beta(1+\lambda d) + \alpha\lambda d}{(1+\alpha)} \right) e^{-\lambda d} \\
\Delta \tilde{u}_{2,1}(\lambda, d) &= \frac{b_2}{\pi} \left(\frac{\alpha(1+\lambda d) - \beta\lambda d}{(1+\alpha)} \right) e^{-\lambda d} \\
\Delta \tilde{u}_{1,1}(\lambda, -c) &= \frac{b_2}{\pi} \left(\frac{-\beta(1+\lambda c) + \alpha\lambda c}{(1+\alpha)} \right) e^{-\lambda c} \\
\Delta \tilde{u}_{2,1}(\lambda, -c) &= \frac{b_2}{\pi} \left(\frac{-\alpha(1+\lambda c) + \beta\lambda c}{(1+\alpha)} \right) e^{-\lambda c}
\end{aligned}\right\} . \tag{B16}$$

After matching the tractions and the displacement gradients at the strip boundaries $x_2 = d$ and $x_2 = -c$, we obtain

$$\begin{pmatrix} \mathbf{M}_1 & \mathbf{M}_2 & 0 \\ \mathbf{M}_3 & 0 & \mathbf{M}_4 \end{pmatrix} \begin{pmatrix} \mathbf{G} \\ \mathbf{H} \\ \mathbf{F} \end{pmatrix} = \begin{pmatrix} \mathbf{w}_1 \\ \mathbf{w}_2 \end{pmatrix} \tag{B17}$$

where

$$\mathbf{F} = \begin{pmatrix} F_1 \\ F_2 \end{pmatrix}, \quad \mathbf{G} = \begin{bmatrix} G_1 \\ G_2 \\ G_3 \\ G_4 \end{bmatrix}, \quad \mathbf{H} = \begin{pmatrix} H_3 \\ H_4 \end{pmatrix}$$

$$\mathbf{w}_1 = -\frac{\mu_2 \Sigma}{2(1-\nu_2)} \frac{e^{-\lambda(H+c)}}{b_2} \begin{bmatrix} 0 \\ 0 \\ \Delta \tilde{u}_{1,1}(\lambda, -c) \\ \Delta \tilde{u}_{2,1}(\lambda, -c) \end{bmatrix}, \quad \mathbf{w}_2 = -\frac{\mu_2 \Sigma}{2(1-\nu_2)} \frac{e^{-\lambda(H+d)}}{b_2} \begin{bmatrix} 0 \\ 0 \\ \Delta \tilde{u}_{1,1}(\lambda, d) \\ \Delta \tilde{u}_{2,1}(\lambda, d) \end{bmatrix} .$$

and $\mathbf{M}_1$, $\mathbf{M}_2$, $\mathbf{M}_3$, $\mathbf{M}_4$ are given by (B12), and $\Delta \tilde{u}_{i,1}$ are given by (B16). Equation (B17) is solved by Gaussian elimination.

Superposition of the solutions to Problems 1 and 2
  The stresses a distance ζ ahead of a dislocation are given by the superposition of the solutions to Problems 1 and 2

$$\sigma_{i2}(\zeta) = \frac{\mu_2}{4\pi(1-\nu_2)} \left(\frac{2b_i}{\zeta} + f_{ij}(\zeta) b_j \right)$$

$$\sigma_{11}(\zeta) = \frac{\mu_2}{4\pi(1-\nu_2)} \left(\frac{2b_2}{\zeta} + g_i(\zeta) b_i \right)$$

where, from (B8), (B9) and (B14)

$$f_{11}(\zeta) = \frac{4\pi(1-\nu_2)}{\mu_2} \int_0^\infty (-D_1 + D_2 + D_3 + D_4) \sin \lambda\zeta \, d\lambda$$

$$f_{21}(\zeta) = \frac{4\pi(1-\nu_2)}{\mu_2} \int_0^\infty (-D_1 - D_3) \cos \lambda\zeta \, d\lambda$$

$$f_{12}(\zeta) = \frac{4\pi(1-\nu_2)}{\mu_2} \int_0^\infty (G_1 - G_2 - G_3 - G_4) \cos \lambda\zeta \, d\zeta$$

$$f_{22}(\zeta) = \frac{4\pi(1-\nu_2)}{\mu_2} \int_0^\infty (-G_1 - G_3) \sin \lambda\zeta \, d\zeta$$

and

$$g_1(\zeta) = \frac{4\pi(1-v_2)}{\mu_2} \int_0^\infty (D_1 - 2D_2 + D_3 + 2D_4) \cos \lambda\zeta \, d\lambda$$

$$g_2(\zeta) = \frac{4\pi(1-v_2)}{\mu_2} \int_0^\infty (G_1 - 2G_2 + G_3 + 2G_4) \sin \lambda\zeta \, d\lambda. \tag{B18}$$

The integrals in (B18) are evaluated numerically.

APPENDIX C: RESULTS FOR $c_I(c/H, \alpha, \beta), c_{II}(c/H, \alpha, \beta)$

$c_I(0.5, \alpha, \beta)$ Accuracy = 0.1% $[c_{II}(0.5, \alpha, \beta) = 0]$

β \ α	−0.9	−0.8	−0.6	−0.4	−0.2	0	0.2	0.4	0.6	0.8	0.9
−0.4	5.20	2.78	1.27								
−0.3	4.90	2.60	1.16	0.622	0.357						
−0.2	4.59	2.41	1.04	0.531	0.277	0.140	0.070				
−0.1	4.26	2.20	0.916	0.437	0.199	0.070	0.002	−0.025	−0.020		
0	3.91	2.00	0.784	0.336	0.118	0	−0.061	−0.086	−0.082	−0.050	−0.021
0.1			0.634	0.228	0.031	−0.072	−0.123	−0.141	−0.132	−0.096	−0.064
0.2					−0.063	−0.150	−0.189	−0.196	−0.179	−0.134	−0.095
0.3							−0.260	−0.255	−0.227	−0.170	−0.123
0.4									−0.278	−0.207	−0.150

$c_I(0.6, \alpha, \beta)$ Accuracy = 0.1%

β \ α	−0.9	−0.8	−0.6	−0.4	−0.2	0	0.2	0.4	0.6	0.8	0.9
−0.4	5.31	2.84	1.30								
−0.3	5.00	2.65	1.18	0.633	0.363						
−0.2	4.68	2.45	1.06	0.540	0.282	0.143	0.071				
−0.1	4.35	2.24	0.933	0.444	0.202	0.071	0.002	−0.026	−0.022		
0	3.99	2.02	0.795	0.342	0.119	0	−0.062	−0.087	−0.083	−0.051	−0.023
0.1			0.644	0.231	0.031	−0.073	−0.125	−0.143	−0.133	−0.098	−0.066
0.2					−0.065	−0.152	−0.191	−0.199	−0.181	−0.136	−0.097
0.3							−0.263	−0.258	−0.229	−0.172	−0.125
0.4									−0.281	−0.209	−0.152

$c_{II}(0.6, \alpha, \beta)$ Accuracy = 0.5%

β \ α	−0.9	−0.8	−0.6	−0.4	−0.2	0	0.2	0.4	0.6	0.8	0.9
−0.4		−0.212	−0.098								
−0.3		−0.245	−0.113	−0.054	−0.020						
−0.2		−0.275	−0.126	−0.060	−0.023	−0.001	0.012				
−0.1		−0.301	−0.138	−0.066	−0.025	−0.001	0.013	0.021	0.023		
0		−0.325	−0.147	−0.070	−0.026	0	0.016	0.024	0.026	0.022	0.017
0.1			−0.155	−0.072	−0.026	0.002	0.019	0.028	0.030	0.026	0.020
0.2					−0.024	0.005	0.023	0.032	0.035	0.030	0.023
0.3							0.029	0.038	0.040	0.034	0.026
0.4									0.047	0.040	0.030

$c_I(0.7, \alpha, \beta)$ Accuracy = 0.1%

β \ α	−0.9	−0.8	−0.6	−0.4	−0.2	0	0.2	0.4	0.6	0.8	0.9
−0.4	5.67	3.03	1.38								
−0.3	5.34	2.83	1.26	0.671	0.383						
−0.2	5.00	2.61	1.13	0.572	0.298	0.150	0.072				
−0.1	4.64	2.39	0.988	0.469	0.213	0.074	0.001	−0.031	−0.029		
0	4.25	2.14	0.839	0.360	0.125	0	−0.065	−0.092	−0.090	−0.060	−0.031
0.1			0.677	0.242	0.032	−0.077	−0.131	−0.150	−0.141	−0.105	−0.072
0.2					−0.070	−0.160	−0.200	−0.207	−0.189	−0.143	−0.103
0.3							−0.274	−0.268	−0.238	−0.179	−0.130
0.4									−0.290	−0.216	−0.156

$c_{II}(0.7, \alpha, \beta)$ Accuracy = 0.5%

β \ α	−0.9	−0.8	−0.6	−0.4	−0.2	0	0.2	0.4	0.6	0.8	0.9
−0.4		−0.448	−0.210								
−0.3		−0.521	−0.243	−0.116	−0.044						
−0.2		−0.585	−0.272	−0.130	−0.050	−0.002	−0.026				
−0.1		−0.643	−0.297	−0.142	−0.055	−0.002	−0.030	0.046	0.050		
0		−0.695	−0.317	−0.150	−0.057	0	0.034	0.053	0.058	0.049	0.037
0.1			−0.332	−0.155	−0.056	0.004	0.041	0.060	0.066	0.056	0.043
0.2				−0.051		0.012	0.050	0.070	0.076	0.065	0.049
0.3							0.063	0.083	0.087	0.074	0.057
0.4									0.102	0.086	0.066

$c_I(0.8, \alpha, \beta)$ Accuracy = 0.1%

β \ α	−0.9	−0.8	−0.6	−0.4	−0.2	0	0.2	0.4	0.6	0.8	0.9
−0.4											
−0.3				0.757	0.429						
−0.2				0.643	0.334	0.165	0.074				
−0.1				0.525	0.238	0.083	−0.002	−0.041	−0.046		
0				0.399	0.139	0	−0.073	−0.105	−0.106	−0.078	−0.049
0.1					0.033	−0.086	−0.145	−0.165	−0.157	−0.120	−0.086
0.2					−0.082	−0.177	−0.219	−0.226	−0.207	−0.157	−0.115
0.3							−0.299	−0.291	−0.257	−0.193	−0.141
0.4									−0.310	−0.230	−0.167

$c_{II}(0.8, \alpha, \beta)$ Accuracy = 0.5%

β \ α	−0.9	−0.8	−0.6	−0.4	−0.2	0	0.2	0.4	0.6	0.8	0.9
−0.4			−0.351								
−0.3			−0.410	−0.200	−0.075						
−0.2			−0.478	−0.230	−0.088	−0.002	0.050				
−0.1			−0.505	−0.250	−0.097	−0.003	0.054	0.084	0.093		
0			−0.542	−0.265	−0.100	0	0.061	0.094	0.104	0.088	0.066
0.1			−0.570	−0.271	−0.097	0.008	0.073	0.107	0.117	0.100	0.076
0.2					−0.087	0.023	0.089	0.125	0.134	0.114	0.087
0.3							0.113	0.148	0.155	0.131	0.100
0.4									0.182	0.152	0.116

$\phi_{II}(\alpha, \beta) + \omega(\alpha, \beta)$ (in radians)

β \ α	−0.8	−0.6	−0.4	−0.2	0	0.2	0.4	0.6	0.8
−0.4	−0.082	−0.019							
−0.2	−0.119	−0.045	−0.011	0.000	−0.011	−0.038			
−0.1	−0.136	−0.057	−0.019	−0.002	−0.003	−0.017	−0.049	−0.121	
0	−0.150	−0.071	−0.028	−0.001	0	−0.007	−0.027	−0.070	−0.153
0.1			−0.038	−0.011	−0.001	−0.001	−0.012	−0.039	−0.091
0.2				−0.004	0.000	−0.004	−0.021	−0.055	
0.4								−0.017	